

$$e^+e^- \rightarrow e^-\bar{\nu}_e u\bar{d}$$

from LEP to linear collider energies

Y. Kurihara^a, D. Perret-Gallix^b, and Y. Shimizu^a

^aNational Laboratory for High Energy Physics,
Oho 1-1, Tsukuba, Ibaraki 305, Japan

^bLaboratoire d'Annecy-le-Vieux de Physique des Particules
(LAPP), B.P. 110, F-74941 Annecy-le-Vieux Cedex, France

Abstract

The complete tree level cross-section for the process $e^+e^- \rightarrow e^-\bar{\nu}_e u\bar{d}$ is computed using the GRACE system, a program package for automatic amplitude calculation. Special attention is brought to the gauge violation problem induced by the finite width of the W -boson. The *preserved gauge scheme* is introduced and an event generator including double-resonant, single-resonant and non-resonant diagrams with no need for a cut on the electron polar angle is built. Below threshold, the single W and non-resonant diagrams give a substantial contribution to the total cross-section, at linear collider energies, the cross-section, for small electron polar angles, is simply dominated by these contributions. Since no cut needs to be applied to the electron, the generator can be used to estimate background for searches involving jets and missing energy. A monojet event rate estimation based on this process at LEP-I energy is discussed.

To be submitted to Physics Letters B.

1 Introduction

Precise event generators for processes involving W , Z , γ and leading to four fermions in the final state are necessary for a good understanding of the three-boson coupling at LEP and at future linear collider C.M. energies. Four-fermion final state can be produced by double (heavy boson) resonant diagrams, single resonant diagrams or non-resonant diagrams. Single W processes include $e^+e^- \rightarrow l^-\bar{\nu}_l W^+$ where $l = e, \mu$. The $l = e$ case differs from the $l = \mu$ one by the existence of the diagrams where γ , Z^0 or even W are exchanged in the t -channel. Most of these diagrams have a γ - γ like behavior such as a strong forward electron peak, the difference lying in the propagator mass and width. These diagrams will be called the t -channel diagrams hereafter in this paper. Since the W -boson is unstable and decays, final state like $e^+e^- \rightarrow e^-\bar{\nu}_e u\bar{d}$ will be actually observed. The diagrams involved in $e^+e^- \rightarrow e^-\bar{\nu}_e u\bar{d}$ can be grouped into the s -channel (Fig.1) and t -channel classes (Fig.2), each group forms a gauge invariant set. In regard to the W -resonance, they can also be characterized as double-resonant, single-resonant, and non-resonant diagrams. The single and non-resonant diagrams play an important role on several studies, including the W mass determination, the anomalous couplings limits and the background estimates in the search of new particles.

Recently event generators for four-fermion (+ photons) processes have been developed [2]. However, in order to cope with the complexity of the calculations, some approximations are always introduced. On the contrary, the GRACE package can automatically produce the complete set of the tree level diagrams involved in the process while taking into account fermion masses.

In a previous work [1], a complete calculation of two typical processes of four-fermion final states in e^+e^- collisions, $e^+e^- \rightarrow e^-\bar{\nu}_e u\bar{d}$ and $e^+e^- \rightarrow \bar{u}d u\bar{d}$, has been presented for the first time. We have pointed out that the single and non-resonant diagrams play an important role below the W -pair threshold. Their contribution, for instance, reaches 27% for the $\bar{u}d u\bar{d}$ process for $\sqrt{s} = 150$ GeV and gives a non-negligible effect even at higher energy (4.4% for $e^-\bar{\nu}_e u\bar{d}$ at $\sqrt{s} = 190$ GeV). Below the threshold only the off-shell double-resonant amplitudes compete with the single- and non-resonant ones, so that the relative contribution of the latter becomes quite large. Besides a set of experimental loose constraints, a cut on the polar angle of the final

electron with respect to the initial electron direction, θ_e , was applied to avoid a significant gauge violation appearing in the subset of γ - W diagrams.

In this paper, we analyze the effect of the gauge violating term due to the finite width of the W -boson. The so-called *preserved gauge scheme* is introduced to overcome this problem. The total $e^+e^- \rightarrow e^-\bar{\nu}_e u\bar{d}$ cross-section from below the W -pair threshold up to linear collider energy, with no cut on the final electron, is presented. As no constraint need to be applied on the electron kinematic, this generator can be used to estimate the background to signal requesting jets and missing energy like the search for new particles. As an example, the contribution of this process for mono-jet production at LEP-I is estimated in the last section of this paper.

2 The GRACE system

The GRACE system [3] has been developed to perform the very lengthy computations involved in the study of high energy reactions. The GRACE package is a complete set of tools for computing tree level processes. All the usual steps occurring in a given computation are covered: from the process specification to the event generator. It is composed of three components: the diagram generator, the matrix element builder using helicity amplitudes from the CHANEL [4] library and the multi-dimensional phase space integration package BASES [5] associated with the event generator SPRING [5].

Fermion masses are properly taken into account in the helicity amplitudes. The boson width is introduced into the gauge propagator when the denominator may vanish for positive squared momentum transfer. A gauge invariance checking program is automatically built by the system.

The results presented hereafter have been obtained using the following set of parameters:

$$\begin{aligned}
 M_Z &= 91.1 \text{ GeV} \\
 \Gamma_Z &= 2.534 \text{ GeV} \\
 \alpha &= 1/137 \\
 \sin^2 \theta_W &= 1 - (M_W^2/M_Z^2) \\
 M_W &= 80 \text{ GeV} \\
 m_u &= m_d = 0.1 \text{ GeV}.
 \end{aligned}$$

The W width is taken from the Particle Data Group Table: $\Gamma_W = 2.25$ GeV. The gauge boson (W, Z) widths are assumed to be constant in the calculation. Furthermore some realistic experimental cuts have been introduced:

$$\left\{ \begin{array}{ll} 0^\circ < \theta_{e^-} < 180^\circ & \text{case - a} \\ 8^\circ < \theta_{e^-} < 172^\circ & \text{case - b} \end{array} \right\}, \quad 8^\circ < \theta_{u,\bar{d}} < 172^\circ, \quad E_{u,\bar{d}} > 1 \text{ GeV}$$

where θ_{e^-} is the final state electron polar angle, measured from the incident e^- beam, $\theta_{u,\bar{d}}$ are the similar angle for the u and \bar{d} quark and $E_{u,\bar{d}}$ are the energies of final u and \bar{d} quarks.

The gauge invariance of the amplitude without particle width is checked numerically by a random selection of the boson gauge parameters at several points of the phase space. The errors are within the precision of the numerical calculation (typically less than $\mathcal{O}(10^{-12})$ in double precision).

3 Effect of the gauge violating term

The violation of the gauge invariance at the tree level is due to the introduction of the W -boson finite width. The first four diagrams in Fig.2, the so-called γ - W diagrams, give the dominant contribution to the t -channel amplitude, the e^- being scattered in the forward direction. Since a large cancellation occurs among γ - W diagrams [6], the gauge violating terms lead to a strongly divergent cross-section at small electron polar angle. It blows up by about six orders of magnitude at $\theta_e \approx 0$ when the width is introduced directly in the propagator (Fig.3, dashed line).

To see how the effect of the gauge violating term arises, we examine the total amplitude of the γ - W diagrams. Since there is only one W propagator whose four-momentum transfer squared is positive, the amplitude without the W -width can be written as:

$$\mathcal{M} = -\frac{e}{k^2} l_\mu T_\mu, \quad (1)$$

$$T_\mu = \frac{r_\mu}{q^2 - M_W^2} + n_\mu, \quad (2)$$

$$l_\mu = \bar{u}(p') \gamma_\nu u(p) [g_{\mu\nu} + (\xi - 1) k_\mu k_\nu / k^2], \quad (3)$$

$$= \bar{u}(p') \gamma_\mu u(p), \quad (4)$$

where $p_\mu(p'_\mu)$ is the four-momentum of the initial (final) electron, $k_\mu = p_\mu - p'_\mu$, the momentum of the virtual photon, q_μ , the W -propagator four-momentum transfer ($q^2 > 0$) and $r_\mu(n_\mu)$, the single-resonant (non-resonant) diagram amplitudes. If the width, Γ_W , is introduced, one obtains:

$$T_\mu \rightarrow T'_\mu = \frac{r_\mu}{q^2 - M_W^2 + iM_W\Gamma_W} + n_\mu \quad (5)$$

$$= \frac{d_\mu + iM_W\Gamma_W n_\mu}{q^2 - M_W^2 + iM_W\Gamma_W}, \quad (6)$$

$$d_\mu = r_\mu + (q^2 - M_W^2)n_\mu. \quad (7)$$

The square of the electron current, after averaged over spin states, is:

$$L_{\mu\nu} = \overline{\sum_{spin} l_\mu l_\nu^*} = 2[p_\mu p'_\nu + p_\nu p'_\mu + \frac{k^2}{2}g_{\mu\nu}]. \quad (8)$$

Then the squared amplitude is given by:

$$|\mathcal{M}|^2 = \frac{2e^2}{(k^2)^2} \frac{(L_{\mu\nu}d_\mu d_\nu^*) + M_W^2\Gamma_W^2(L_{\mu\nu}n_\mu n_\nu^*)}{(q^2 - M_W^2)^2 + M_W^2\Gamma_W^2}, \quad (9)$$

(note that r_μ and n_μ are real numbers at the tree level). The first term in numerator is the gauge invariant part; when $k^2 \rightarrow 0$, it behave as $L_{\mu\nu}d_\mu d_\nu^* \rightarrow \mathcal{O}(k^2)$. The second term is the gauge violating one as $L_{\mu\nu}n_\mu n_\nu^* \rightarrow \mathcal{O}(1)$ when $k^2 \rightarrow 0$. By integrating over k^2 , the former gives the well-known $\log(s/m_e^2)$ dependence of the total cross-section. The latter, the gauge violating term, however, dominates the total cross-section after integration, as it does not compensate the photon propagator $\propto 1/(k^2)^2$. It is clear that this term is responsible for the divergence of the cross-section in the small angle region (Fig.3, dashed line). It should be emphasized that this behavior does not depend on the gauge parameter of the W propagator.

The introduction of the W width, yet preserving the gauge invariance of the amplitude, can be achieved by applying the following method.

The current l_μ is replaced by the momentum k_μ , gauge invariance implies:

$$k_\mu T_\mu = \frac{k \cdot r}{q^2 - M_W^2} + k \cdot n, \quad (10)$$

$$= \frac{k \cdot d}{q^2 - M_W^2} = 0. \quad (11)$$

Then d_μ is a gauge invariant quantity. T_μ can be expressed in term of d_μ as:

$$T_\mu = \frac{d_\mu}{q^2 - M_W^2}. \quad (12)$$

If the particle width is introduced at this stage, the amplitude can be cast into the form:

$$T_\mu \rightarrow T_\mu'' = \frac{d_\mu}{q^2 - M_W^2 + iM_W\Gamma_W}. \quad (13)$$

This amplitude is apparently gauge invariant as the divergent term discussed previously has disappeared [8]. The total cross-sections based on this amplitude do not diverge even in the small angle region as shown by the solid line in Fig.3. This scheme, the *preserved gauge scheme*, can be interpreted as follows; the tree-level amplitude is gauge invariant but divergent at $q^2 = M_W^2$. To avoid this divergence, an imaginary part of a higher-order is introduced into the propagator denominator as a particle width. However this order mixing causes the violation of the gauge invariance at the tree-level and gives rise to the cross-section divergence. To preserve the gauge invariance, an additional term is added to the amplitude on the analogy of the counterterms, it gives the higher order correction to the leading term.

In order to check the validity of the method, one can approach this result by applying a method which minimize the gauge violating term. Let us remind a usual trick used for the tensor $L_{\mu\nu}$. Let's assume, first, that T_μ is gauge invariant. One can replace $L_{\mu\nu}$ by:

$$L_{\mu\nu} \rightarrow L'_{\mu\nu} = 4p_\mu p_\nu + k^2 g_{\mu\nu}. \quad (14)$$

In this equation, the first term is responsible for the blow-up of the cross section. Because of the gauge invariance, one can further replace the vector p_μ by:

$$p_\mu \rightarrow P_\mu = p_\mu - (p_0/k_0)k_\mu, \quad (15)$$

where p_0 and k_0 are the 0-th components of the four-momenta p_μ and k_μ , respectively. By substituting p_μ in Eq.(15) and dropping k_μ , one gets

$$L'_{\mu\nu} \rightarrow L''_{\mu\nu} = 4P_\mu P_\nu + k^2 g_{\mu\nu}. \quad (16)$$

It is known that a product $P \cdot A$ of P with an arbitrary vector A can be expressed by a sum of terms proportional to either m_e^2 , $1 - \cos \theta_e$ or $\sin \theta_e$.

Hence in the region $\theta_e \approx 0$, both $P \cdot d$ and $P \cdot n$ behave like k^2 , because $1 - \cos \theta_e$ vanishes almost like k^2 .

Then, one possible way to get rid of the large gauge violation is to use the current $L''_{\mu\nu}$, instead of the original one $L_{\mu\nu}$ in Eq.(9). The new amplitude squared becomes:

$$|\mathcal{M}|^2 \rightarrow \frac{2e^2}{(k^2)^2} \frac{(L''_{\mu\nu} d_\mu d_\nu^*) + M_W^2 \Gamma_W^2 (L''_{\mu\nu} n_\mu n_\nu^*)}{(q^2 - M_W^2)^2 + M_W^2 \Gamma_W^2}. \quad (17)$$

The gauge violating term $L''_{\mu\nu} n_\mu n_\nu$ behaves as $\mathcal{O}(k^2)$ for vanishing k^2 , and it should not induce violent divergence. Since the non-resonant diagrams have a W -boson space-like propagator, one may assume roughly that $\mathcal{O}(r_\mu) \sim \mathcal{O}(n_\mu M_W^2)$. Hence the gauge violating term is proportional to $(\Gamma_W/M_W)^2 \sim 10^{-3}$. This is small compared to the gauge invariant term $(L''_{\mu\nu} d_\mu d_\nu^*)$ and can be neglected.

Using this last method, the cross-section turns out to be 8.63×10^{-2} pb (case-a at $\sqrt{s} = 180$ GeV) as seen in Fig.3 (indicated by the arrow). This is only 5% larger than the cross-section obtained by the *preserved gauge scheme* (8.24×10^{-2} pb).

4 Threshold behavior

In the following, the computations are performed using the *preserved gauge scheme*. The contribution from the t -channel diagrams strongly depends on θ_e cut as shown in Fig.4. If we require the electron polar angle to be in the range $172^\circ > \theta_e > 8^\circ$ (140 mrad) case-b, the double-resonant diagrams are dominant (96% at $\sqrt{s} = 180$ GeV) but their contributions are reduced down to 83% if the electron angular cut is set to a vanishing value (case-a).

The threshold behavior of $e^+e^- \rightarrow e^- \bar{\nu}_e u \bar{d}$ total cross-section is presented in Fig.5 together with one high energy point ($\sqrt{s} = 500$ GeV). With no electron angular cut, case-a, one observes a large increase in the cross-section due to the t -channel diagrams, although when such a cut is applied, case-b, the effect remains substantial only above threshold. The relative contribution of the double-resonant diagrams is shown in Fig.6. At $\sqrt{s} = 500$ GeV, the share of the double-resonant diagrams is only 17% without electron tagging (case-a), while it amounts to 55% when the electron is tagged (case-b).

For the W mass measurement, it should be noted that using the threshold scanning method, a precise electron tagging is necessary to deal with the t -channel contribution. When the direct reconstruction of 2-jets is used, the invariant mass distribution of a quark pair gets a low mass tail from the non-resonant diagrams. The effect of the electron angular cut is to suppress the contribution from those diagrams, as shown in Fig.7.

In the studies of the anomalous couplings of the gauge bosons, the process $e^+e^- \rightarrow e\nu_e W$ is considered. However the process to be measured is $e^+e^- \rightarrow e\nu_e q\bar{q}$ [7] which includes the effect of the non-resonant diagrams. The contributions of t -channel diagrams (Fig.2) have been computed for both processes $e^+e^- \rightarrow e\nu_e W$ and $e^+e^- \rightarrow e\nu_e q\bar{q}$, with no cut, a 14% discrepancy is found in the total cross-section at $\sqrt{s} = 180$ GeV, which comes from the small angle region of the final electron.

$$1 - \frac{\sigma(ee \rightarrow e\nu W) * Br(W \rightarrow ud)}{\sigma(ee \rightarrow e\nu ud)} = 0.14$$

This effect should definitely be taken into account in these studies.

The *preserved gauge scheme* can also be applied to different processes, like those appearing at electron-electron collider. For example, the process $e^-e^- \rightarrow e^-W^-\nu_e$ [9] involves only the t -channel diagrams at the tree level.

A comparison with the four-fermion Monte-Carlo EXCALIBUR [10] has been performed for the $e^+e^- \rightarrow e^-\bar{\nu}_e u\bar{d}$ channel as an independent test of our work. However such a comparison make sense only when a cut is applied on the electron polar angle as EXCALIBUR does not treat the forward divergence. Under this condition, perfect agreement is obtained with our generator without the *preserved gauge scheme*. Identical divergent behavior is found when the cut is decreased down to almost zero. The net result of our study is the extension of the domain of validity of the generator for massive fermions and for vanishing electron polar angle.

5 Monojet event rate at LEP

The ALEPH collaboration at LEP has reported the observation of three monojet events, one leptonic and two hadronic, from a data sample of $82 pb^{-1}$ [11] recorded at and close to the Z^0 peak. Although the event rate is consistent with the expectation from $e^+e^- \rightarrow \gamma^*\nu\bar{\nu}$ with $\gamma^* \rightarrow f\bar{f}$, the large

observed monojet mass and transverse momentum are quite unlikely in this process. Even when diagrams from Z or W exchanges are taken into account, the probability of their occurrence is about 5%.

For the W exchange process, $e^+e^- \rightarrow e\nu f\bar{f}'$, only four types of diagrams are taken into account, double-resonant and single-resonant diagrams in s -channel and single-resonant diagrams in t -channel. Non-resonant diagrams were not included as no generator was available at that time. These diagrams are expected to give a large contribution to the total cross-section at energies below the W -pair threshold, moreover the mass and transverse momentum distribution are expected to peak at higher values.

The expected number of events from $e^+e^- \rightarrow e^\pm(\bar{\nu}_e)q\bar{q}'$ and the probability to produce the observed jet masses and transverse momenta have been estimated by applying the ALEPH cuts at the generator level.

1. $\theta_e < 25$ mrad.
2. Polar angle of $q\bar{q}'$ system $< 25.8^\circ$.
3. Neither q nor \bar{q}' goes backward of $q\bar{q}'$ system.
4. $E_{q\bar{q}'} > 1.3$ GeV.

The total cross-section of the $e^+e^- \rightarrow e^\pm(\bar{\nu}_e)q\bar{q}'$ processes ($q\bar{q}' = u\bar{d}$ and $c\bar{s}$) at $\sqrt{s} = 91.1$ GeV with the above cuts is 7.2×10^{-3} pb, which corresponds to 0.59 events for a integrated luminosity of 82 pb $^{-1}$. The expected event distribution of $q\bar{q}'$ invariant masses and transverse momenta are shown in Figs.8 and 9, respectively with the same binning as Fig.3 in ref.[11]. The observed jet masses and transverse momenta of the hadronic monojet ($M = 3.2, 5.3$ GeV and $p_T = 6.6, 18.5$ GeV) are distributed around the peak of the distributions. The probability defined in ref.[11] is calculated to be 0.95. The observed events are compatible with the expectation obtained from $e^+e^- \rightarrow e^\pm(\bar{\nu}_e)q\bar{q}'$ processes. However detailed calculations with hadronization and detector simulation are needed to give a more precise estimation.

6 Summary and Conclusions

The complete tree level cross-section of the process $e^+e^- \rightarrow e^-\bar{\nu}_e u\bar{d}$ has been computed using the GRACE package. It is shown that the naive method of

introducing the W width induces an unphysical divergent total cross-section due to the gauge violation among the t -channel tree-level diagrams. This effect is sizable when the electron scattering angle is less than a few degrees. Two *ad hoc* methods are discussed, one curing definitely the violent blow up of the amplitude (the *preserved gauge scheme*) and the other strongly reducing this violation.

The cross-sections as a function of the CM energies without any cut on the final electron are presented. We conclude that the approximation based only on a part of the diagrams (the double-resonant diagrams and/or the single-resonant γ - W diagrams) is not sufficient to give precise predictions neither at threshold energy nor at high energy. For the W mass determination based on the W pair threshold scanning, the complete calculation should be used and a precise measurement of the electron should be made. The single-resonant diagrams can be used for the W mass measurement by the 2 jet reconstruction method, although the kinematic constraints are much weaker. Observed jet masses and transverse momenta of hadronic monojet seen by the ALEPH collaboration at LEP are not in contradiction with the expectation from $e^+e^- \rightarrow e^\pm(\bar{\nu}_e)q\bar{q}'$ processes when naive experimental cuts are applied at parton level.

Acknowledgment

We would like to thank our colleagues in Minami-Tateya theory group of KEK and those in LAPP for valuable discussions and encouragement. Particularly we are indebted to T. Kaneko, H. Tanaka and T. Ishikawa for their help in GRACE system and S. Kawabata for providing a high quality diagram drawing package. We would like also to thank J. Kubo, I. Ginzburg and F. Cuypers for fruitful discussions on the treatment of the particle width.

This work has been done in the framework of the KEK-LAPP collaboration supported in part by the Ministry of Education, Science and Culture(Monbusho) under the Grant-in-Aid for International Scientific Research Program No.04044158 in Japan and by le Centre National de la Recherche Scientifique (CNRS/IN2P3) in France.

References

- [1] T. Ishikawa, T. Kaneko, S. Kawabata, Y. Kurihara, Y. Shimizu, H. Tanaka, KEK Preprint 92-210.
- [2] H. Anlauf, P. Manakos, T. Mannel, H.D. Dahmen, IKDA 93/28,SI 93-4, hep-ph/9308237,
D. Bardin, M. Bilenky, D. Lehner, A. Olchevski, T. Riemann, CERN-TH.7295/94, DESY 94-093,
G.J. van Oldenborgh, PSI-PR-94-06,
F.A Berends, R. Pittau, R. Kleiss, INLO-PUB-1/94, NIKHEF-H/94-08.
- [3] T. Ishikawa, T. Kaneko, K. Kato, S. Kawabata, Y. Shimizu and H. Tanaka, KEK Report 92-19, 1993, The GRACE manual Ver. 1.0
- [4] H. Tanaka, *Comput. Phys. Commun.* **58** (1990) 153
and see also H. Tanaka, T. Kaneko and Y. Shimizu, *Comput. Phys. Commun.* **64**(1991) 149.
- [5] S. Kawabata, *Comput. Phys. Commun.* **41**(1986) 127.
- [6] E.E. Boos, M. Sachwitz, H.J. Schreiber, S. Shichanin, A. Pukhov, V. Ilyin, T. Ishikawa, T. Kaneko, S. Kawabata, Y. Kurihara, Y. Shimizu, H Tanaka, *Phys. Lett.* **B326** (1994) 190.
- [7] E.N. Argyres, C.G. Papadopoulos, *Phys. Lett.* **B263** (1991) 298,
Y. Miyamoto, in the *Proceedings of the 2nd International Workshop on Physics and Experiments with Linear e^+e^- Colliders*, Waikoloa, Hawaii, 1993,
C.G. Papadopoulos, *Phys. Lett.* **B333** (1994) 202.
- [8] This scheme is equivalent to the scheme proposed by A.E. Pukhov and V. Ilyin (private communication), and the *overall scheme* in A. Aeppli, F. Cuypers, G.J. van Oldenborgh, TTP92-36, PSI-PR-93-05, LMU-21/92. See also U. Baur, J.A.M. Vermaseren, D. Zeppenfeld, *Nucl. Phys.* **B375** (1992)3.
- [9] V. Barger, J.F. Beacom, K. Cheung, and T. Han University of Wisconsin Madison Mad/ph/779.

[10] EXCALIBUR, F.A Berends, R. Pittau, R. Kleiss, INLO-PUB-1/94, NIKHEF-H/94-08.

[11] ALEPH Collaboration, *Phys. Lett.* **B334** (1994) 244.

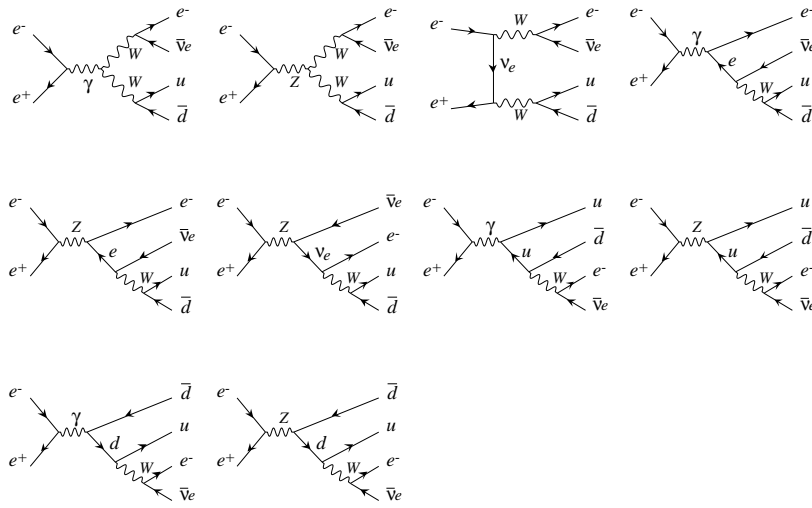


Figure 1: The s -channel diagrams of the $e^+e^- \rightarrow e^-\bar{\nu}_e u\bar{d}$ process in unitary gauge. The first three diagrams in the first row are double-resonant diagrams.

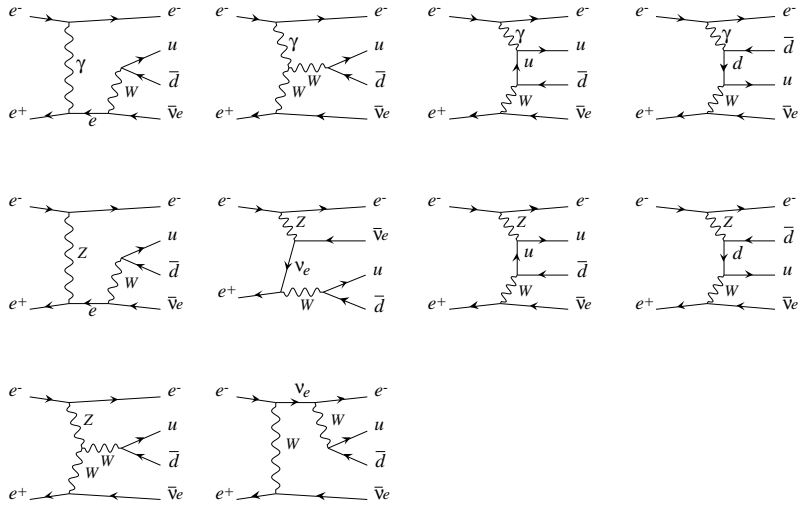


Figure 2: The t -channel diagrams of $e^+e^- \rightarrow e^-\bar{\nu}_e u\bar{d}$ process in unitary gauge. The first and second columns show the single-resonant diagrams and the rest shows the non-resonant diagrams. Diagrams in first row (γ - W processes) give the dominant contribution among t -channel diagrams.

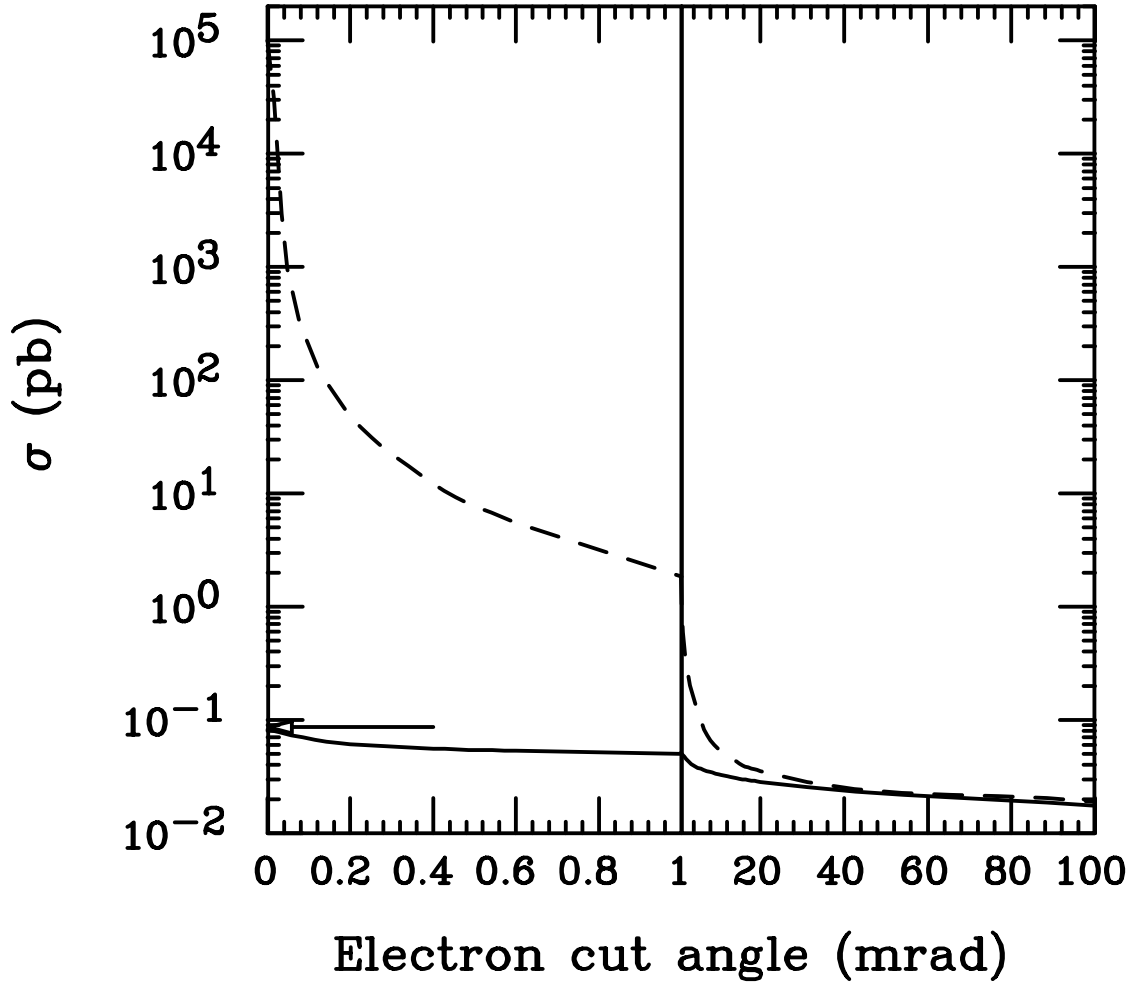


Figure 3: The cross-section vs. electron cut angle for the sub-set of γ - W diagrams only at $\sqrt{s} = 180$ GeV. The left half of the figure is a magnified view of the small angle region. The dashed line shows a result with a naive Breit-Wigner form for the W -propagator and the solid line corresponds to the introduction of the width in a gauge-invariant way using the so-called *preserved gauge scheme* as explained in the text. The arrow shows the cross-section using the second method described in the section 3.

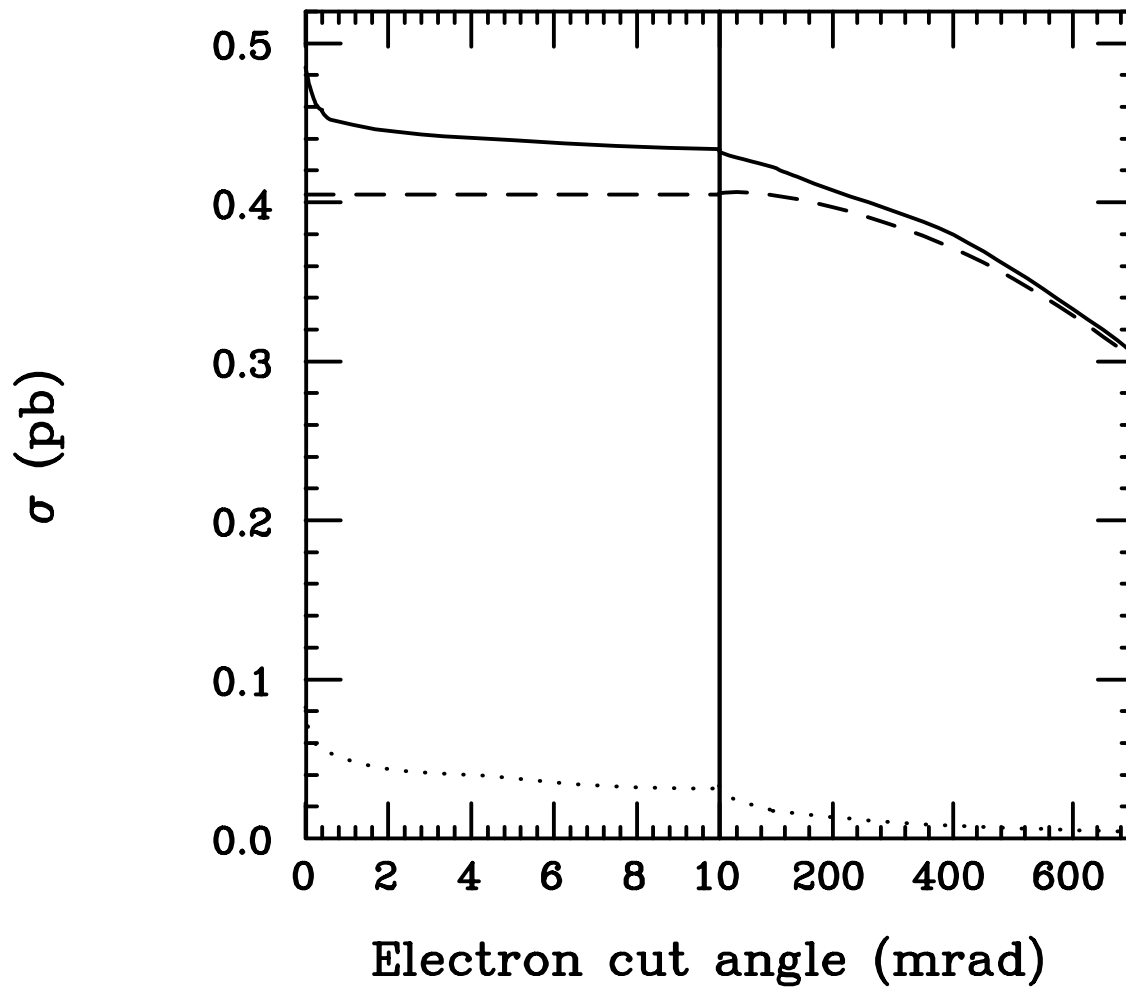


Figure 4: The cross-section vs. the e^- cut angle at $\sqrt{s} = 180$ GeV. The solid line represents the contribution from all diagrams, the dashed line from the double-resonant diagrams, and the dotted line from the γ - W diagrams.

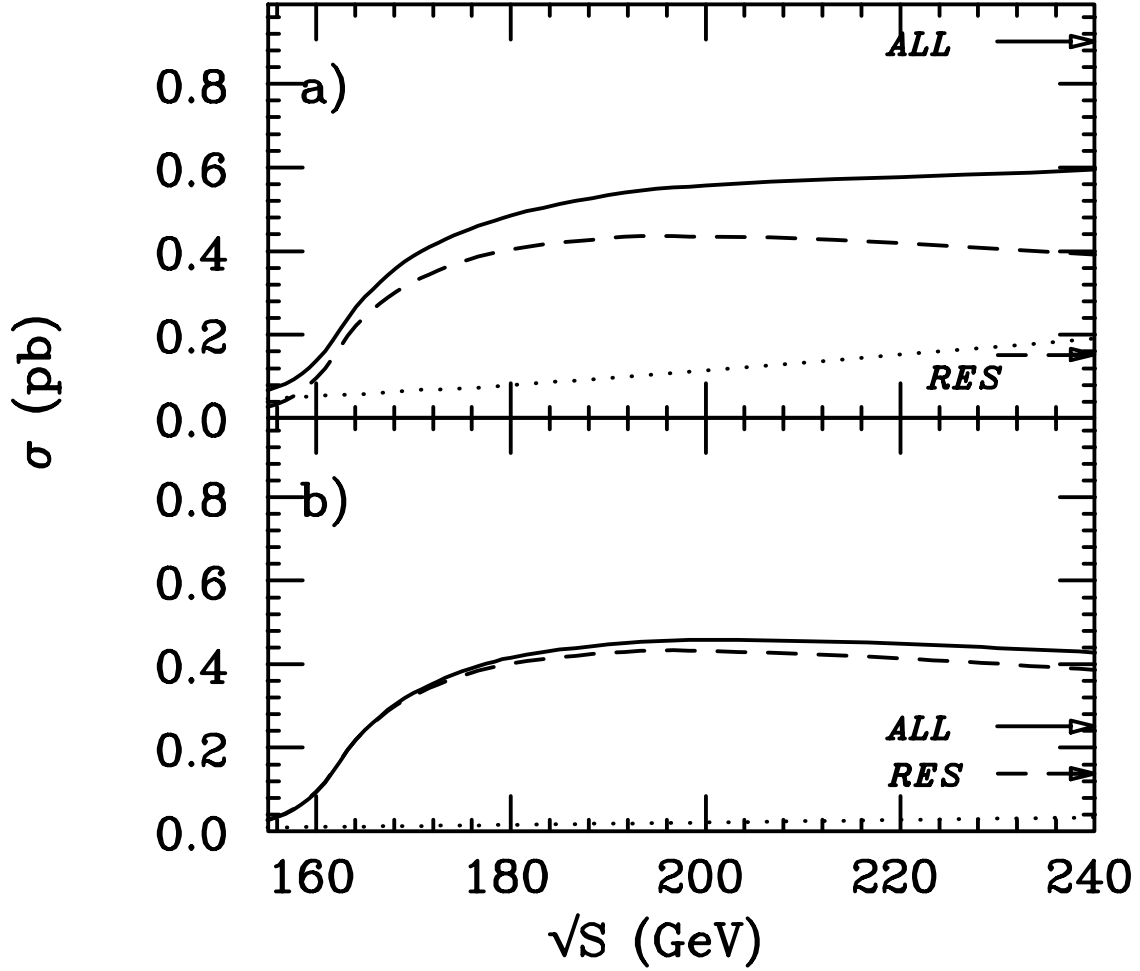


Figure 5: The threshold behavior of the total cross-section of the $e^+e^- \rightarrow e^-\bar{\nu}_e u\bar{d}$ process. Cuts described in section 2 are applied on u and \bar{d} quarks, a) no cut on the final electron (case-a), and b) $\theta_e > 8^\circ$ (case-b). The solid line shows the cross-section from all diagrams, the dashed line from the double-resonant diagrams, and the dotted line from the t -channel diagrams. Results at $\sqrt{s} = 500$ GeV are shown by solid arrows (all diagrams) and dashed arrows (double-resonant diagrams).

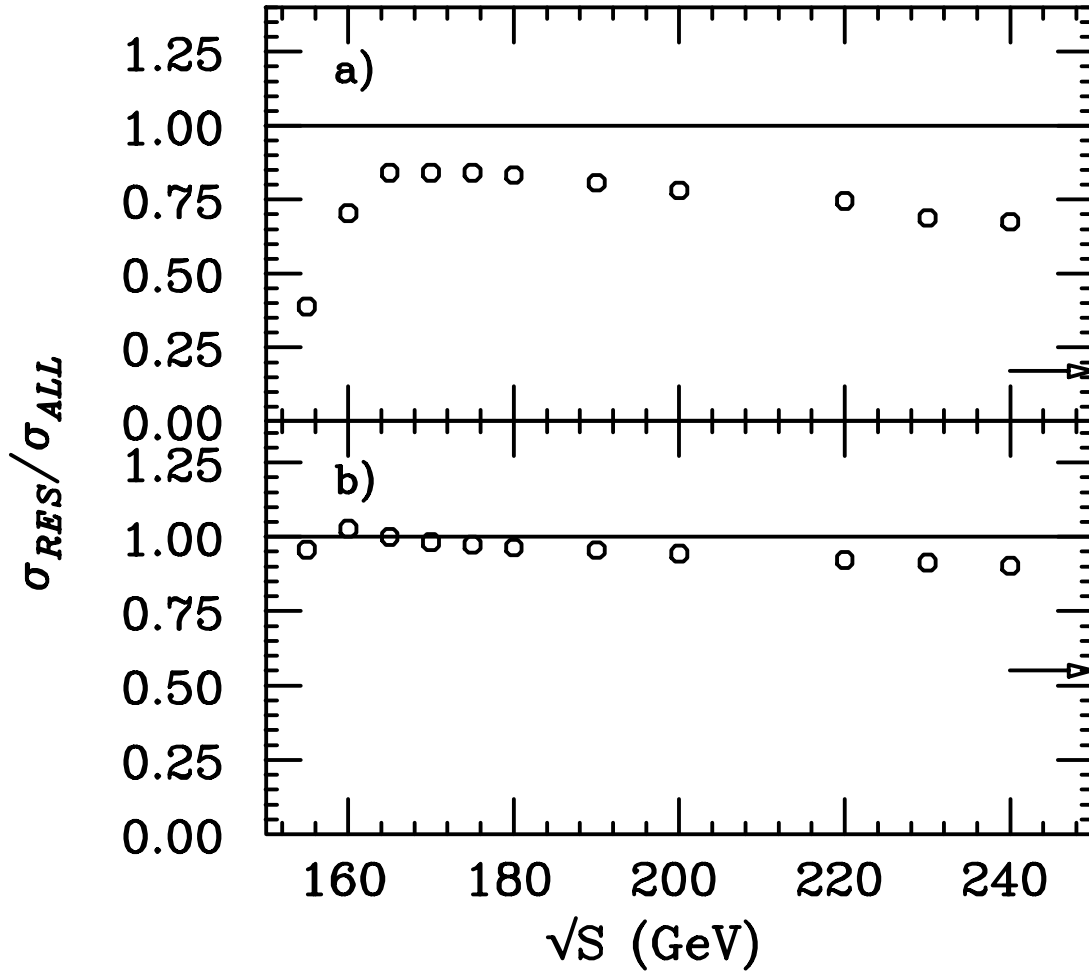


Figure 6: The relative contribution of the double-resonant diagrams to the cross-sections at $\sqrt{s} = 180$ GeV. In a), no cut on the out-going electron but only on u and \bar{d} (case-a) and in b) an additional cut, $\theta_e > 8^\circ$ (case-b), is imposed. Results at $\sqrt{s} = 500$ GeV are shown by arrows.

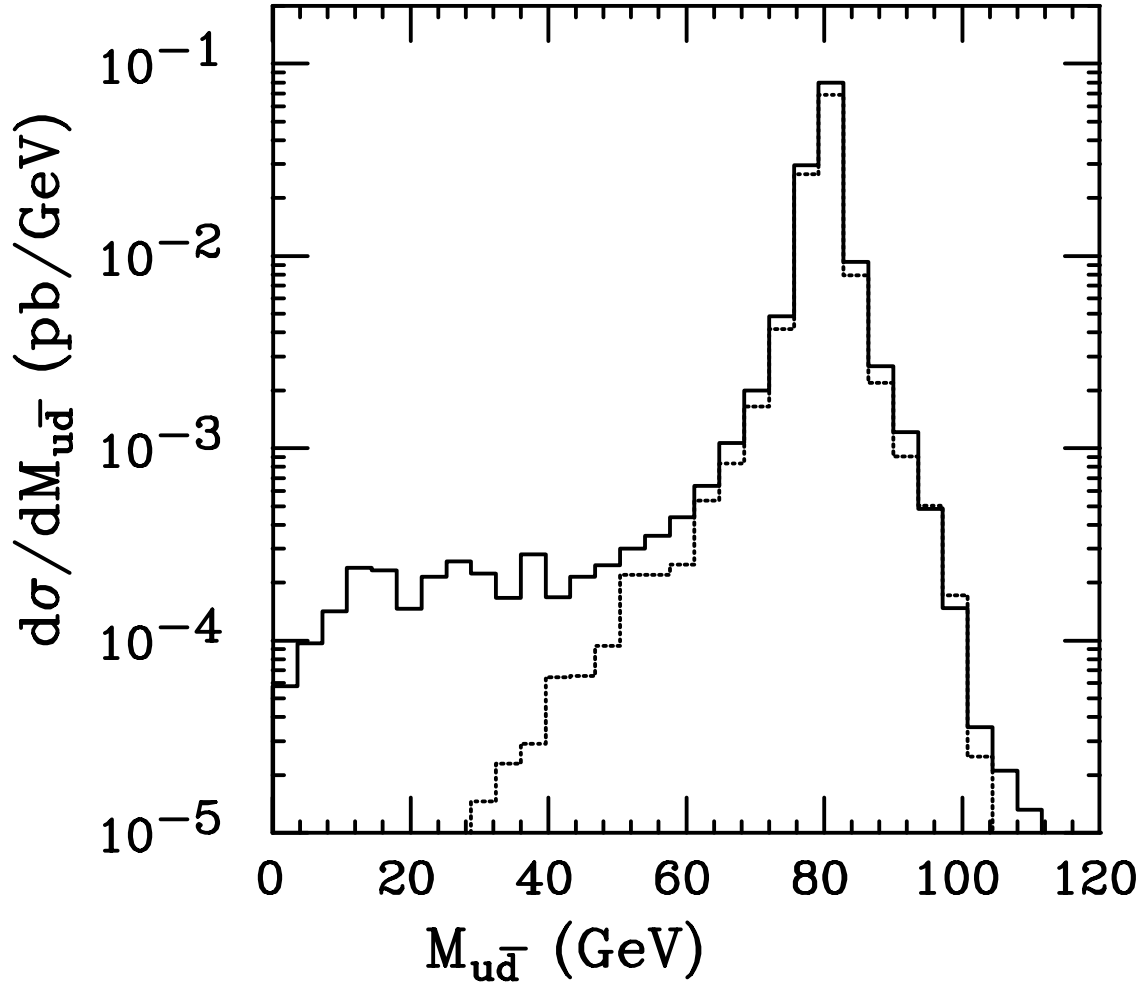


Figure 7: The invariant mass distribution of u and \bar{d} calculated at $\sqrt{s} = 180$ GeV. The solid line (case-a), and the dotted one with additional cut, $\theta_e > 8^\circ$ (case-b).

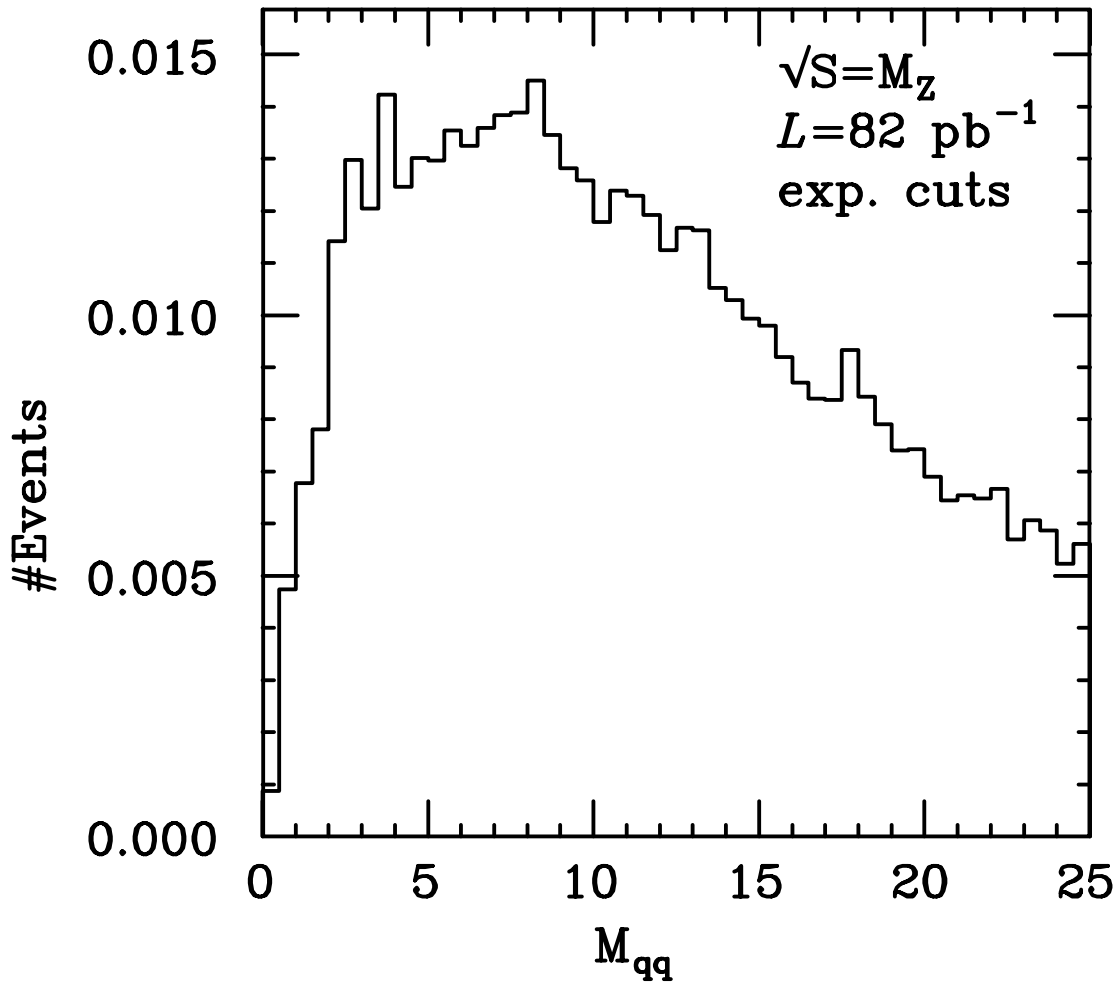


Figure 8: The invariant mass distribution of q and \bar{q}' calculated at $\sqrt{s} = M_Z$. The integrated luminosity and experimental cuts described in ref.[11] but applied at the generator level is assumed.

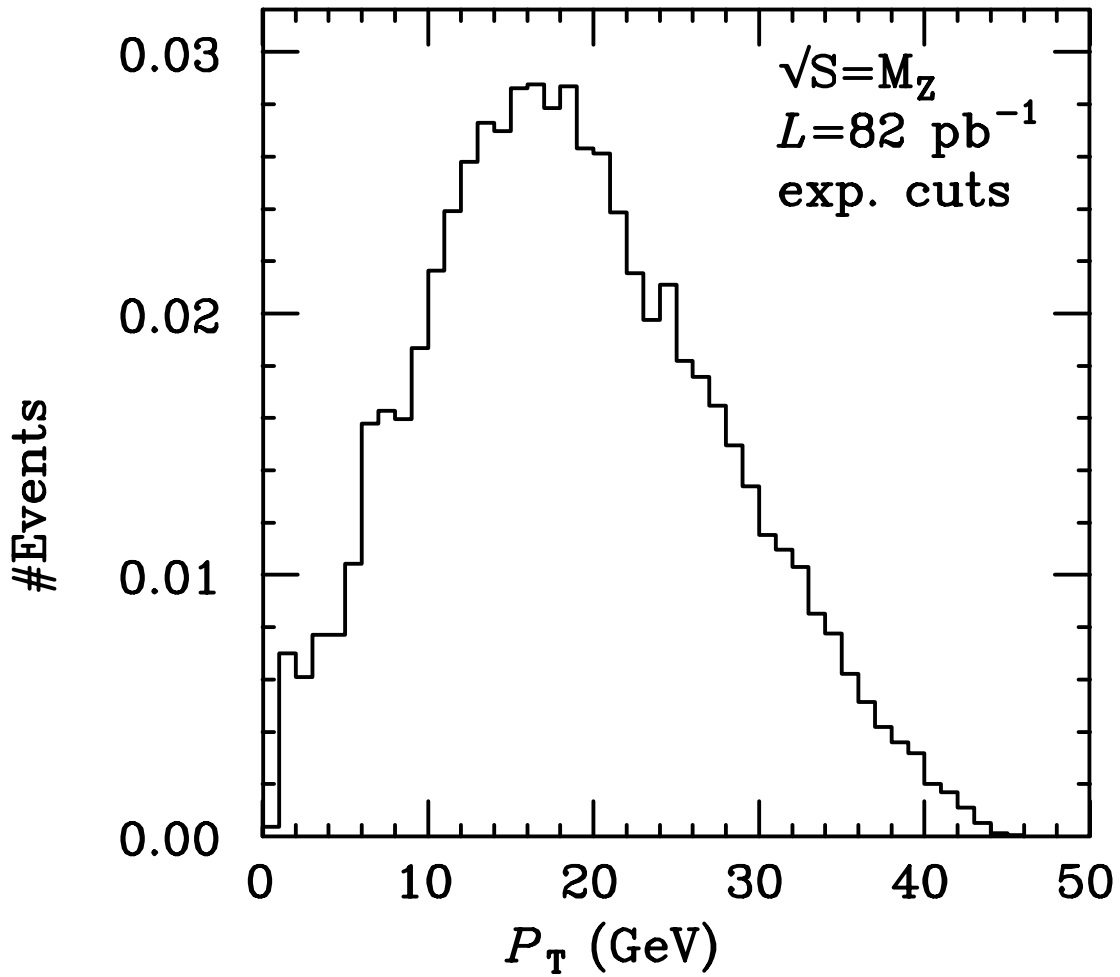


Figure 9: The transverse momentum of $q\bar{q}'$ system calculated at $\sqrt{s} = M_Z$. The integrated luminosity and experimental cuts described in ref.[11] but applied at the generator level are assumed.

